

RESEARCH ARTICLE

MMP-2 associated imbalance of VEGF/Endostatin is linked to suppression of the PI3K/AKT/HIF-1 α pathway in steroid-induced osteonecrosis of femoral head

Guangyang Zhang, Zhaopu Jing, Jialin Liang, Leifeng Lv, Xiaoqian Dang*, Qichun Song *

Department of Sports Medicine, Orthopedic Center, the Second affiliated hospital of Xi'an Jiaotong University, Xi'an, Shaanxi, China

* dangxiaoqian@xjtu.edu.cn (XD); qichuns@xjtu.edu.cn (QS)



 OPEN ACCESS

Citation: Zhang G, Jing Z, Liang J, Lv L, Dang X, Song Q (2026) MMP-2 associated imbalance of VEGF/Endostatin is linked to suppression of the PI3K/AKT/HIF-1 α pathway in steroid-induced osteonecrosis of femoral head. PLoS One 21(4): e0346880. <https://doi.org/10.1371/journal.pone.0346880>

Editor: Xindie Zhou, The Affiliated Changzhou No 2 People's Hospital of Nanjing Medical University, CHINA

Received: September 18, 2025

Accepted: March 17, 2026

Published: April 17, 2026

Copyright: © 2026 Zhang et al. This is an open access article distributed under the terms of the [Creative Commons Attribution License](https://creativecommons.org/licenses/by/4.0/), which permits unrestricted use, distribution, and reproduction in any medium, provided the original author and source are credited.

Data availability statement: All relevant data are within the paper and its [Supporting information](#) files.

Funding: This study was supported by the Fundamental Research Funds for the Central

Abstract

Objective

To investigate the role of matrix metalloproteinase-2 (MMP-2) and the imbalance between vascular endothelial growth factor (VEGF) and Endostatin in the pathogenesis of steroid-induced osteonecrosis of femoral head (SONFH).

Methods

Clinical samples and animal models were combined to systematically analyze the impact of VEGF/Endostatin imbalance on angiogenesis and osteogenesis. Clinical samples from SONFH patients and femoral neck fracture controls were analyzed for VEGF, Endostatin and MMP-2 expression. The SONFH model in C57BL/6J mice was established to evaluate the effects of an imbalanced VEGF/Endostatin axis on angiogenesis and osteogenesis, assessed by micro-CT based vascular imaging, calcein labeling, and bone density analysis. MMP-2 intervention experiments were conducted to explore its role in the VEGF/Endostatin ratio.

Results

Clinical data revealed significantly lower VEGF/Endostatin ratio ($P < 0.001$) and higher MMP-2 levels ($P < 0.05$) in necrotic regions of SONFH patients compared to the controls. In animal models, decreased VEGF/Endostatin ratio caused by Endostatin supplementation could further suppress angiogenesis and osteogenesis ($P < 0.05$). Mechanistically, MMP-2 disrupts the VEGF/Endostatin balance by decreasing VEGF expression ($P < 0.05$) and increasing Endostatin levels ($P < 0.05$), which is associated with the suppression of PI3K/AKT/HIF-1 α pathway.

Universities (grant number xzy012025125) awarded to Q.C.S. The funder is the Fundamental Research Funds for the Central Universities. Funder website: <https://www.moe.gov.cn/>. The funder had no role in study design, data collection and analysis, decision to publish, or preparation of the manuscript.

Competing interests: The authors have declared that no competing interests exist.

Conclusions

Our findings reveal that the imbalance of VEGF/Endostatin is a key driver of SONFH through impaired angiogenesis and osteogenesis. We further demonstrate that MMP-2 contributes to this imbalance, likely linked to suppression of the PI3K/AKT/HIF-1 α pathway. These results support the VEGF/Endostatin ratio as a potential diagnostic biomarker and suggest that targeting MMP-2 or Endostatin may represent promising therapeutic strategies.

1. Introduction

Osteonecrosis of the femoral head (ONFH) is a common disabling orthopedic disorder characterized by the interruption of blood flow to the femoral head, finally resulting in necrosis of bone cells and marrow elements. This pathophysiological process eventually leads to femoral head collapse, joint dysfunction, and the need for total hip arthroplasty [1]. Among the various etiologies of ONFH, steroid-induced osteonecrosis of the femoral head (SONFH) represents one of the most prevalent forms [2]. Since the first clinical report in 1953 linking corticosteroid therapy with femoral head necrosis, the incidence of SONFH has significantly increased, largely due to the extensive use of glucocorticoids in managing autoimmune diseases, transplantation, and severe infections [3]. Although the mechanisms of SONFH are multifactorial, accumulating evidence highlights that impaired angiogenesis during bone remodeling is a critical pathological feature that drives disease progression [4,5]. During the early stages of osteonecrosis, ischemia and hypoxia damage osteocytes and stromal components. If timely neovascularization and osteogenesis occur, necrotic tissue may be replaced and remodeled. However, if angiogenic repair fails, progressive bone deterioration and structural collapse ensue. Therefore, elucidating the regulation of angiogenesis in SONFH is essential for understanding its pathogenesis and developing novel therapeutic strategies.

Vascular endothelial growth factor (VEGF) plays a central role in the initiation and maintenance of angiogenesis. As a pro-angiogenic factor, VEGF promotes endothelial cell proliferation, migration, and new vessel formation [6]. Reduced VEGF expression has been associated with impaired blood supply and delayed bone repair in ONFH. Several experimental studies have shown that VEGF delivery or gene therapy can effectively improve neovascularization and accelerate bone regeneration in osteonecrotic lesions [7]. In contrast, Endostatin, an endogenous angiogenesis inhibitor derived from collagen XVIII, antagonizes VEGF signaling by inhibiting endothelial proliferation and promoting vessel regression [8]. While Endostatin has been extensively studied in tumor biology, its role in SONFH remains insufficiently defined and potentially detrimental. Our previous work in a rabbit SONFH model demonstrated that exogenous Endostatin administration significantly exacerbates bone necrosis and reduces neovascular formation [9], suggesting that anti-angiogenic stress may play a negative role in this context.

The ratio of VEGF to Endostatin expression may thus represent a valuable index reflecting the balance between pro- and anti-angiogenic forces within various diseases. For example, operable non-small cell lung cancer patients have been shown to exhibit a higher VEGF/Endostatin ratio than healthy controls, and this imbalance is associated with poorer prognosis [10]. Additionally, it was revealed that the dynamic changes of VEGF and Endostatin illustrate a shifting angiogenic balance that contributes to hepatocellular carcinoma progression and may hold diagnostic and prognostic value [11]. Furthermore, Ai Jing et al. reported that restoring the VEGF/Endostatin balance by elevating Endostatin levels effectively ameliorated pathological retinal neovascularization [12]. However, the dynamic regulation of this ratio and its pathological consequences in SONFH have yet to be fully clarified. Notably, matrix metalloproteinases (MMPs), particularly MMP-2, are implicated in extracellular matrix remodeling and may indirectly affect the bioavailability and activity of angiogenic factors. MMP-2 is known to degrade extracellular matrix (ECM) components, modulate cytokine gradients, and potentially alter VEGF storage or release, thereby influencing angiogenic potential [13]. Previous research found that MMP-2, VEGF and Endostatin all played critical roles in the healing of NSAID induced small intestinal ulcers in rats [14]. Additionally, Sara A et al. demonstrated that the expression of VEGF, Endostatin, and MMP-2 undergone a complex and tightly coordinated regulation in response to both acute and chronic exercise training in mice [15]. However, the role of MMP-2 in affecting VEGF and Endostatin expression during SONFH remains unexplored. Moreover, identifying early molecular changes in SONFH is critical for timely diagnosis and intervention. While magnetic resonance imaging remains the clinical gold standard for detecting early stage SONFH, it lacks molecular specificity. Therefore, investigating the potential of VEGF/Endostatin ratio as a serum or tissue biomarker may provide a novel avenue for early detection or risk stratification.

In this study, we combined clinical sample analysis with a steroid-induced mouse model of femoral head to investigate the expression pattern and functional implications of the VEGF/Endostatin axis. We further explored the involvement of MMP-2 in disturbing this balance and assessed its impact on angiogenesis and osteogenesis. Through this integrative approach, we aim to clarify the molecular mechanisms underlying impaired vascular remodeling in SONFH and propose novel targets for early diagnosis and therapeutic modulation.

2. Materials and methods

2.1 Clinical samples

From January 1, 2023 to December 31, 2023, patients diagnosed with SONFH (ARCO stage III–IV) were enrolled as the experimental group, while age, sex, and BMI matched patients undergoing total hip arthroplasty for femoral neck fracture served as the control group with approval from the Ethics Committee of the Second Affiliated Hospital of Xi'an Jiaotong University (Approval No. 2022194). Patients were eligible for inclusion when they met all of the following criteria: age 18–65 years; a clinical and radiological diagnosis of steroid-induced osteonecrosis of the femoral head according to accepted diagnostic criteria; ARCO stage III–IV disease at the time of enrollment; no prior surgical intervention on the affected hip; and the ability to provide written informed consent and comply with study procedures. Patients were excluded if any of the following applied: osteonecrosis due to trauma, alcohol abuse, metabolic bone disease, hemoglobinopathy, or other non-steroidal causes; prior hip surgery, hip infection, or malignant disease involving the hip; systemic conditions likely to confound outcomes (such as severe hepatic or renal failure, uncontrolled diabetes, or active systemic infection); use of investigational drugs within three months prior to enrollment; or inability to provide informed consent or comply with follow-up. All procedures were conducted in accordance with the Declaration of Helsinki. All participants provided written permission for publication, and informed consent was collected from each individual. The femoral head specimens were collected intraoperatively, fixed in 4% paraformaldehyde for 48 hours, decalcified in 10% EDTA solution for four weeks, dehydrated through graded ethanol, and embedded in paraffin for subsequent histopathological analysis.

2.2 Animal models

The study was approved by the Biomedical Ethics Committee of Xi'an Jiaotong University Health Science Center (Approval No. XJTUAE2025–2549). Forty-eight eight-week-old male C57BL/6J mice were used, and the modeling period lasted eight weeks. Mice were housed in standard cages with appropriate bedding, ambient temperature 22 ± 2 °C, 12:12 h light: dark cycle, ad libitum access to food and water, and provided nesting material for enrichment. Mice were monitored daily for health and welfare and weighed weekly. Predefined humane endpoints included $\geq 20\%$ body weight loss, inability to eat or drink, severe or progressive lameness preventing normal feeding or mobility, severe respiratory distress, or moribund state. Animals meeting humane endpoint criteria were euthanized promptly (≤ 4 h after detection) by overdose of pentobarbital sodium (100 mg/kg, intraperitoneally; Sigma-Aldrich) with confirmation of death. After a 7-day acclimatization period, the mice were randomly divided into four groups: control, SONFH, SONFH with MMP-2 supplementation (SONFH+MMP-2), and SONFH with Endostatin supplementation (SONFH+Endostatin). The SONFH model was induced by intraperitoneal injection of lipopolysaccharide (20 $\mu\text{g}/\text{kg}$; Sigma-Aldrich, Missouri, USA) on two consecutive days, followed by daily intramuscular injections of methylprednisolone (100 mg/kg; Sigma-Aldrich, Missouri, USA) into the gluteus maximus for 14 days, then continued every other day [16]. Mice were simultaneously subjected to elevated feeding to encourage upright posture and rotating cage exercise of 2 h/day to increase activity. Mice in the SONFH+MMP-2 group received subcutaneous injections of recombinant MMP-2 (10 $\mu\text{g}/\text{kg}$; MedChemExpress, NJ, USA) every three days [17,18], while those in the SONFH+Endostatin group were administered daily subcutaneous injections of recombinant Endostatin (2 mg/kg; MedChemExpress, NJ, USA) [9]. The control group received equivalent volumes of physiological saline throughout the experiment. All procedures were conducted by trained personnel. The steroid-induced model did not involve surgical procedures. Animals were handled gently to minimize stress. No routine peri-procedural analgesia was required, but any animal showing signs consistent with pain or distress received rescue analgesia per veterinary instruction. Scheduled euthanasia by overdose of pentobarbital sodium (100 mg/kg, intraperitoneally; Sigma-Aldrich) at 8 weeks was performed identically and bilateral femoral heads were harvested and frozen in liquid nitrogen for subsequent analysis. No unplanned or spontaneous deaths occurred during the study.

2.3 Hematoxylin and eosin, immunofluorescence staining

Mouse femoral head specimens were fixed in 4% paraformaldehyde for 48 hours, followed by decalcification in 10% EDTA solution at 37 °C with gentle agitation. The decalcification solution was refreshed every 3 days until the tissue was fully softened. After routine paraffin embedding, serial sections were prepared for hematoxylin and eosin (HE) staining to observe bone tissue structure.

As for the Immunofluorescence staining, paraffin sections were deparaffinized, subjected to antigen retrieval, and blocked with 5% goat serum. Sections were then incubated overnight at 4 °C with primary antibodies against VEGF and Endostatin. After washing, sections were incubated for 1 hour at room temperature in the dark with FITC- or Cy3-conjugated secondary antibodies, followed by nuclear counterstaining with DAPI. The slides were mounted and imaged using a fluorescence microscope.

2.4 Micro-computed tomography and micro-computed tomography–based angiography

Following euthanasia, femoral heads were harvested from C57BL/6J mice, fixed in 4% paraformaldehyde for 48 hours, and then immersed in 75% ethanol for micro-computed tomography (micro-CT) scanning. The scanning was performed using a Bruker Skyscan system under the following parameters: 70 kV voltage, 200 μA current, 10 μm resolution, 525 ms exposure time, and 180° rotation angle. A calibration phantom was scanned simultaneously for standardization. The raw images were reconstructed using NRecon software (version 1.7.4.2, Bruker), and the following parameters were analyzed using CT Analyser software (version 1.18.8.0, Bruker): bone mineral density (BMD), trabecular number (Tb.N),

trabecular thickness (Tb.Th), trabecular separation (Tb.Sp), bone volume (BV), and the bone surface-to-bone volume ratio (BS/BV).

For vascular imaging, mice were anesthetized and perfused via the left ventricle with heparinized saline followed by 4% paraformaldehyde, and subsequently with Microfil contrast agent at a flow rate of 3 mL/min. The aorta was ligated, and the specimens were kept at 4 °C overnight. The femurs were then harvested, fixed in 4% paraformaldehyde for 24 hours, decalcified in 10% EDTA, and scanned using Micro-CT. Scanning parameters were set as follows: 70 kV voltage, 200 μ A current, 6.5 μ m resolution, 525 ms exposure time, and 180° rotation angle. Calibration with a phantom was performed concurrently. The reconstructed images were used to analyze vascular volume fraction using the same software and methodology.

2.5 Calcein staining

Dynamic bone formation in the femoral head was evaluated using Calcein staining. In the sixth week of modeling, mice received an intraperitoneal injection of Calcein (10 mg/kg, dissolved in 2% NaHCO₃ solution; MedChemExpress, NJ, USA), followed by a second injection 6 days later. After euthanasia, femoral heads were harvested, fixed in 4% paraformaldehyde for 48 hours, and dehydrated through a graded ethanol series. Specimens were then embedded in methyl methacrylate, and continuous sections were prepared. Hard tissue microtome was used for precise sectioning, and calcein fluorescence signals were acquired using a laser scanning confocal microscope. The mineral apposition rate (MAR) was quantitatively analyzed to assess the rate of new bone formation.

2.6 Quantitative real-time polymerase chain reaction

Total RNA was isolated from femoral head samples using TRIzol reagent (Thermo Fisher Scientific, MA, USA) following the manufacturer's instructions. The concentration and purity of RNA were determined with a NanoDrop spectrophotometer (Invitrogen, USA). Subsequently, complementary DNA (cDNA) was synthesized using the PrimeScript RT Master Mix (Takara, Japan) according to the standard protocol. Quantitative real-time PCR (RT-qPCR) was carried out using SYBR Select Master Mix (Vazyme, Nanjing, China) on a CFX96 real-time PCR detection system (Bio-Rad, Hercules, USA). GAPDH was used as the internal reference gene, and relative mRNA expression levels were calculated using the 2^{- $\Delta\Delta$ Ct} method. Primer sequences are listed in [S1 Table](#).

2.7 Western blotting

Proteins were extracted from femoral head tissues using a standard lysis protocol, and total protein concentrations were determined using a BCA Protein Assay Kit (Beyotime, Shanghai, China). Equal amounts of protein were subjected to SDS-PAGE and subsequently transferred onto 0.22 μ m PVDF membranes (Millipore, USA). Membranes were blocked with 5% non-fat milk at room temperature for 2 hours and then incubated overnight at 4 °C with primary antibodies (1:1000 dilution). After washing, the membranes were incubated with horseradish peroxidase (HRP)-conjugated secondary antibodies (1:5000 dilution) for 1 hour at room temperature. Protein bands were visualized using an enhanced chemiluminescence detection kit (Millipore, USA), and the grayscale intensity of each band was quantified using ImageJ software. Detailed information on the antibodies used is provided in [S2 Table](#).

2.8 Statistical analysis

Statistical analyses were conducted using SPSS 23.0 (IBM) and GraphPad Prism 9.0. Continuous data are expressed as mean \pm SD. Comparisons between two groups used independent t-tests, while categorical variables were analyzed with Chi-square test. Multigroup comparisons employed one-way ANOVA (parametric method) based on normality assessment, with post hoc testing where appropriate. Statistical significance was set at P < 0.05.

3. Results

3.1 The VEGF/Endostatin ratio decreases but MMP-2 increases in SONFH patients

To investigate angiogenic and anti-angiogenic factors in SONFH, femoral head samples were collected from patients with steroid-induced osteonecrosis. Samples from patients undergoing femoral head replacement for femoral neck fractures were collected as controls. Following routine fixation, decalcification, and paraffin embedding, immunofluorescence was performed to assess VEGF and Endostatin expression. As shown in Fig 1A–1D, the SONFH group exhibited a marked reduction in VEGF expression compared to the control group ($P < 0.01$), alongside a significant increase in Endostatin levels ($P < 0.01$). Consequently, the VEGF/Endostatin ratio was significantly lower in osteonecrotic femoral heads than in controls (2.991 ± 0.113 vs 0.283 ± 0.098 ; $P < 0.001$). Additionally, the level of MMP-2 in the femoral heads was detected by Western blotting method. As shown in Fig 1E and 1F, MMP-2 expression was significantly increased in the SONFH groups compared with the control group ($P < 0.05$). These findings suggest that the pathological progression of osteonecrosis is closely associated with a disturbed balance of VEGF/Endostatin ratio and MMP-2 expression.

3.2 Establishment of a SONFH mouse model and angiogenesis assessment

To further explore the mechanisms underlying impaired angiogenesis in osteonecrosis, particularly the imbalance between pro- and anti-angiogenic factors, a steroid-induced osteonecrosis model was established in 8-week-old male C57BL/6 mice. Macroscopic observation revealed that femoral heads in all groups maintained smooth surfaces and regular shapes, with no apparent collapse. Histological examination via HE staining (Fig 2A) revealed preserved trabecular architecture, rich hematopoietic marrow, and few adipocytes in the control group. In contrast, SONFH mice demonstrated sparse, irregular, and fractured trabeculae, disrupted marrow hematopoiesis, and increased adipocyte infiltration. Notably, further elevation of anti-angiogenic pressure through Endostatin supplementation aggravated these histopathological alterations, accompanied by more pronounced nuclear pyknosis, karyorrhexis, and the appearance of empty osteocyte lacunae (red arrows). The percentage of empty osteocytes was quantified and is shown in Fig 2B. Compared with the control group, the SONFH group exhibited a significant increase in the percentage of empty osteocytes ($P < 0.0001$), which was further increased upon Endostatin supplementation ($P < 0.01$).

Additionally, micro-CT-based angiography was conducted to evaluate vascular numbers and density (Fig 2C). Quantitative analysis revealed a significant reduction in vascular volume fraction in the SONFH group compared to the controls (Fig 2E, $P < 0.001$). Endostatin supplementation further suppressed vascular formation ($P < 0.001$), suggesting that a shift toward an anti-angiogenic balance markedly impairs femoral head angiogenesis under pathological conditions.

3.3 Altered osteogenic phenotypes following Endostatin supplementation in the femoral head

Calcein staining was then used to assess the effect of Endostatin supplementation on osteogenesis by measuring the mineral apposition rate (MAR). Compared with controls, SONFH mice displayed a narrower inter-label distance and reduced MAR (Fig 2D and 2F; $P < 0.05$), and Endostatin supplementation further diminished mineralization capacity ($P < 0.05$), consistent with a further perturbation of the osteogenic microenvironment.

To validate these findings, micro-CT was used to assess bone architecture, including BMD, Tb.N, Tb.Th, Tb.Sp, BV, and BS/BV (Fig 3A). The SONFH group exhibited a marked reduction in BMD relative to controls (Fig 3B; $P < 0.0001$), which was exacerbated by Endostatin supplementation ($P < 0.001$). Similarly, Tb.N, Tb.Th, and BV were all significantly decreased following Endostatin supplementation (Fig 3C, 3D and 3F; $P < 0.05$). In contrast, Tb.Sp did not differ significantly between control and SONFH groups (Fig 3E; $P > 0.05$); Endostatin supplementation had no effect on Tb.Sp compared with SONFH alone, although Tb.Sp remained higher than in controls ($P < 0.05$). The BS/BV ratio mirrored the pattern observed for Tb.Sp: Endostatin supplementation increased BS/BV relative to controls (Fig 3G; $P < 0.05$), but no differences were detected between control versus SONFH or SONFH versus SONFH+Endostatin. Together, these data

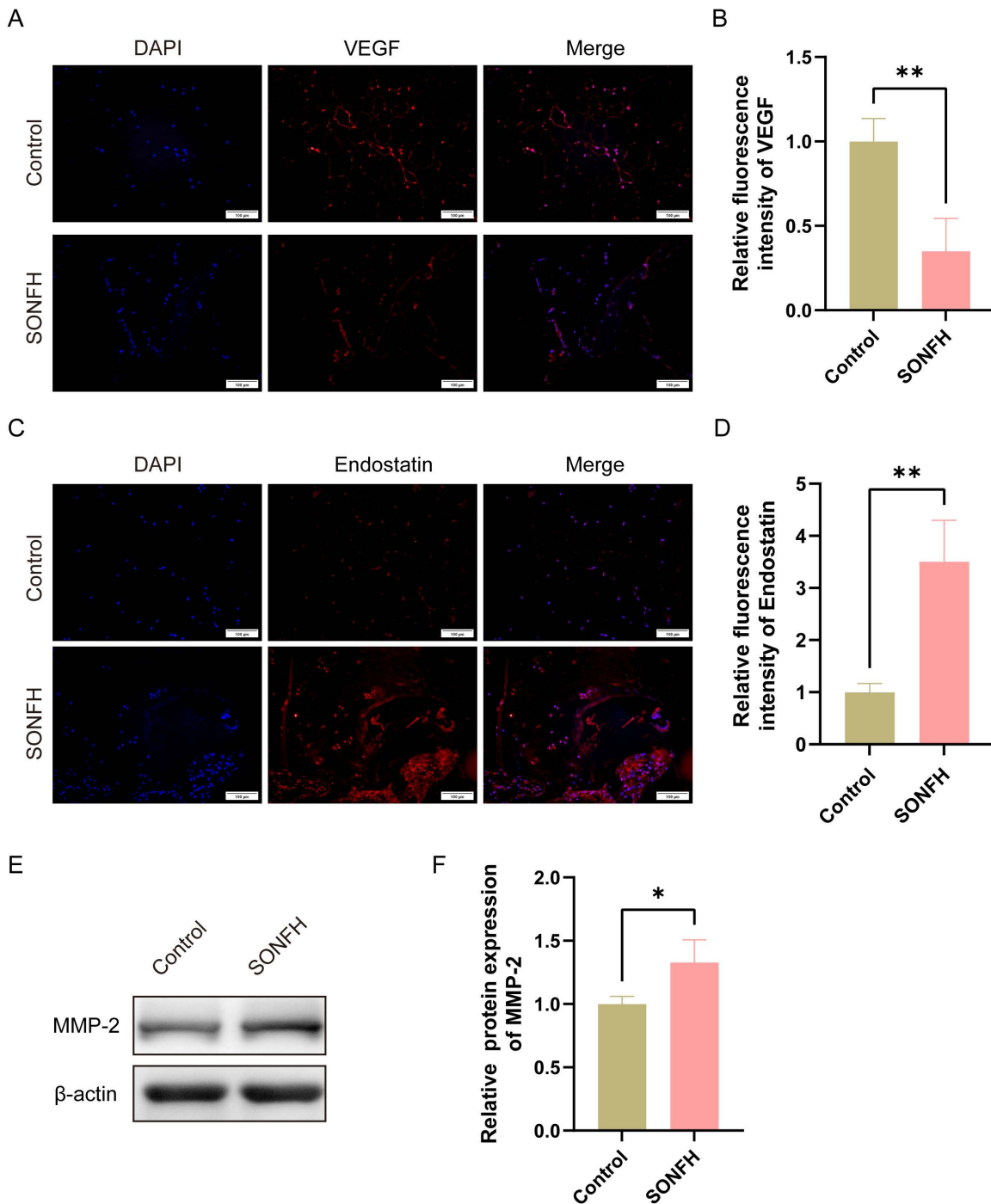


Fig 1. Expression changes of VEGF/Endostatin and MMP-2 in the femoral head of SONFH patients. (A) Representative immunofluorescence images showing VEGF expression in the femoral head of control and SONFH groups (scale bar=100 μm); (B) Quantification of VEGF fluorescence intensity in control and SONFH groups; (C) Representative immunofluorescence images showing Endostatin expression in the femoral head of control and SONFH groups (scale bar=100 μm); (D) Quantification of Endostatin fluorescence intensity in these two groups; (E) Representative Western blotting images of MMP-2 expression in the femoral head of control and SONFH groups; (F) Quantification of MMP-2 expression in these two groups. (*P<0.05, **P<0.01).

<https://doi.org/10.1371/journal.pone.0346880.g001>

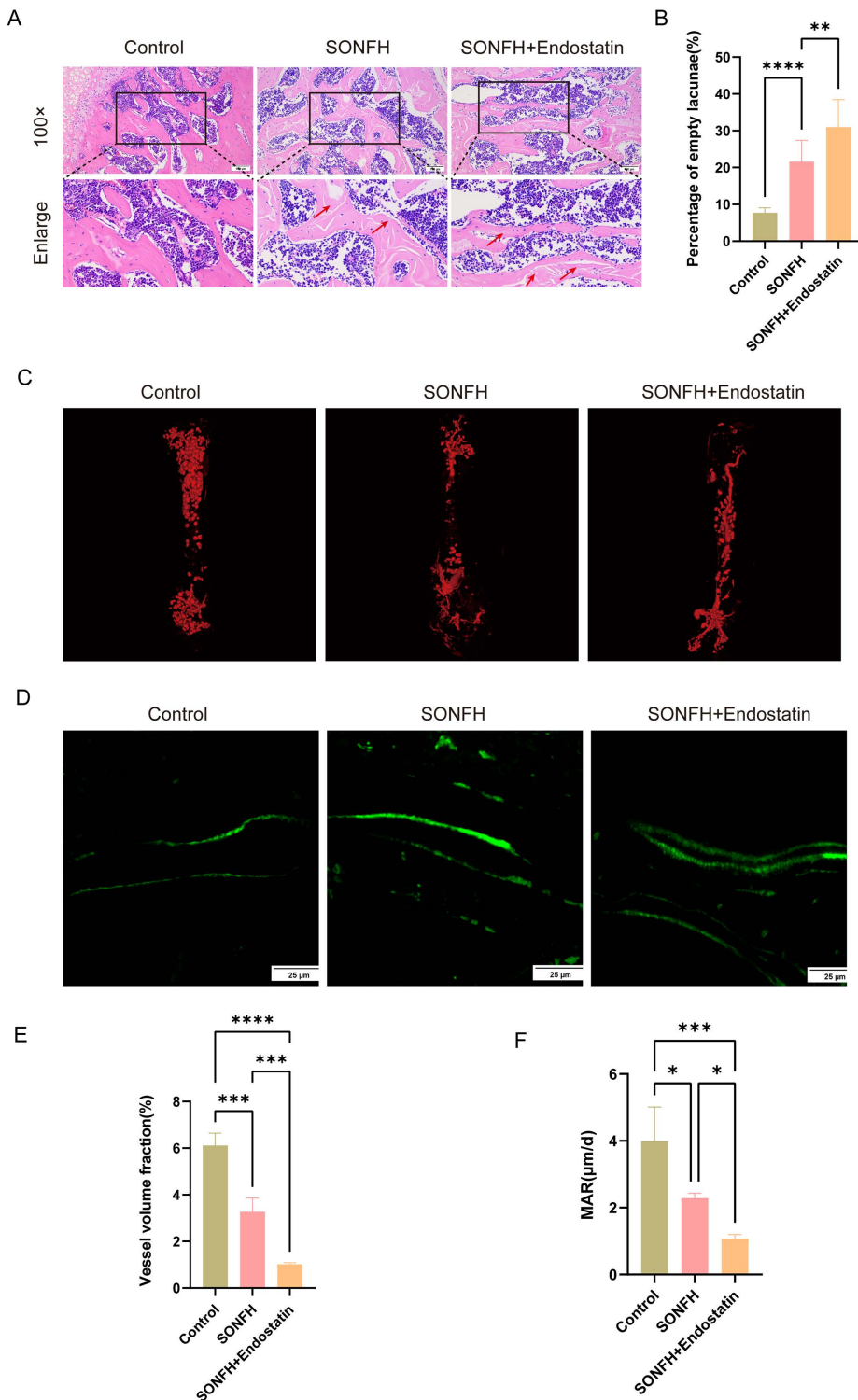


Fig 2. Angiogenic and osteogenic phenotypic changes following Endostatin supplementation in the femoral head of mice. (A) Representative HE staining images of the femoral head in control, SONFH, and SONFH+Endostatin groups (scale bar=100 μm); (B) Quantitative analysis of percentage of empty osteocyte from HE staining; (C) Representative micro-CT vascular reconstructions of the femoral head in each group; (D) Calcein staining images showing mineral apposition in each group (scale bar=25 μm); (E) Quantitative analysis of vascular volume fraction from micro-CT angiography; (F) Quantification of mineral apposition rate (MAR) in each group. (*P<0.05, ***P<0.001, ****P<0.0001).

<https://doi.org/10.1371/journal.pone.0346880.g002>

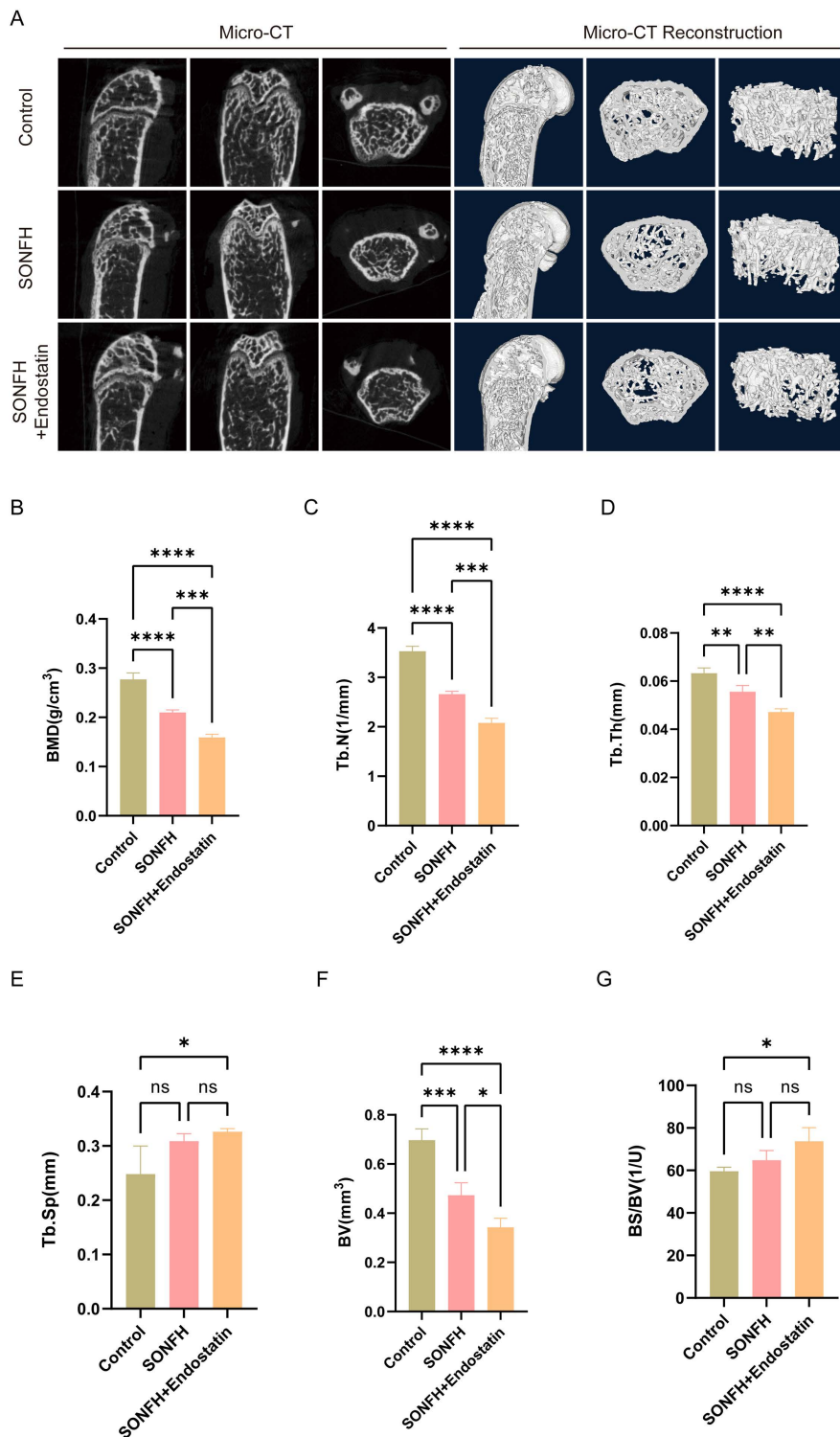


Fig 3. Micro-CT analysis of femoral heads in different experimental groups. (A) Representative micro-CT images of femoral heads; (B) Quantitative analysis of bone mineral density (BMD); (C) Quantification of trabecular number (Tb.N); (D) Quantification of trabecular thickness (Tb.Th); (E) Quantification of trabecular separation (Tb.Sp); (F) Quantification of bone volume (BV); (G) Quantification of the bone surface-to-bone volume ratio (BS/BV). (BMD: bone mineral density; Tb.N: trabecular number; Tb.Th: trabecular thickness; Tb.Sp, trabecular separation; BV, bone volume; BS/BV, bone surface-to-bone volume ratio. (*P<0.01, ***P<0.001, ****P<0.0001).

<https://doi.org/10.1371/journal.pone.0346880.g003>

demonstrate that Endostatin supplementation exacerbates disruption of the osteogenic microenvironment and adversely affects bone remodeling in the femoral head. These osteogenic impairments are consistent with the detrimental effects on angiogenesis observed earlier, highlighting the coupled nature of vascular and bone remodeling processes in SONFH.

3.4 MMP-2 decreases VEGF level but enhances Endostatin expression and may contribute to osteonecrosis progression

To elucidate the role of MMP-2 in affecting angiogenic factors during steroid-induced osteonecrosis of the femoral head, mice were randomized into four groups: control, SONFH, SONFH+Endostatin, and SONFH+MMP-2. We first confirmed MMP-2 expression by Western blotting. Compared with controls, MMP-2 protein levels were significantly elevated in the SONFH group (Fig 4A, 4B; $P < 0.01$). Exogenous MMP-2 supplementation further increased MMP-2 expression in the femoral head ($P < 0.001$), whereas Endostatin supplementation had no appreciable effect on MMP-2 levels ($P > 0.05$).

Next, we assessed VEGF expression at both the mRNA and protein levels. RT-qPCR revealed a marked reduction in VEGF mRNA in the SONFH group relative to controls ($P < 0.0001$). Supplementation with either Endostatin or MMP-2 resulted in additional downregulation of VEGF mRNA ($P < 0.05$), implicating the role of MMP-2 in VEGF suppression during osteonecrosis. Consistent with these findings, Western blotting and immunofluorescence analyses demonstrated significantly lower VEGF protein in SONFH femoral heads (Fig 4E and 4G; $P < 0.01$), with further suppression upon Endostatin and MMP-2 supplementation ($P < 0.01$ and $P < 0.05$, respectively). No significant difference was observed between the Endostatin and MMP-2 supplementation groups. Collectively, these data indicate that MMP-2, like Endostatin, critically contributes to angiogenic insufficiency in SONFH by downregulating VEGF.

Moreover, to determine whether MMP-2 also influences Endostatin expression, we measured Endostatin levels in all groups by RT-qPCR, Western blotting, and immunofluorescence. Endostatin mRNA was significantly upregulated in the SONFH group versus controls (Fig 5A; $P < 0.01$), but remained unchanged following MMP-2 supplementation ($P > 0.05$), suggesting that MMP-2 does not directly regulate Endostatin transcription. Western blotting confirmed increased Endostatin protein in SONFH mice (Fig 5B; $P < 0.01$). And MMP-2 supplementation modestly elevated Endostatin protein levels ($P < 0.01$), while exogenous Endostatin supplementation also significantly enhanced endogenous Endostatin levels ($P < 0.01$), suggesting a potential additive or feedback mechanism. Immunofluorescence mirrored these results, showing that Endostatin expression was higher in the SONFH group compared to controls (Fig 5C; $P < 0.001$) and was further increased in both MMP-2 and Endostatin intervened mice ($P < 0.05$). Together, these findings indicate that although MMP-2 does not transcriptionally modulate Endostatin, it may potentiate Endostatin protein accumulation through other mechanisms. Additionally, we calculated the VEGF/Endostatin ratio according to the immunofluorescence results. The control group had a ratio of 1.840 ± 0.597 , whereas the SONFH group was significantly lower (0.303 ± 0.024 ; $P < 0.05$). Further decreases were observed in the SONFH+MMP-2 (0.054 ± 0.015) and SONFH+Endostatin (0.087 ± 0.023) groups compared with the SONFH group ($P < 0.001$ and $P < 0.01$, respectively). No significant difference was found between the SONFH+MMP-2 and SONFH+Endostatin groups ($P > 0.05$). Taken together, these findings indicate that the detrimental effects of Endostatin supplementation are mediated not by Endostatin alone, but by a shift toward an anti-angiogenic VEGF/Endostatin balance.

3.5 MMP-2 is linked to suppression of PI3K/AKT/HIF-1 α pathway

As the PI3K/AKT/HIF-1 α pathway is essential for both angiogenesis and osteogenesis, we hypothesized that MMP-2 disrupts the VEGF/Endostatin balance by suppressing this signaling pathway. We therefore measured key pathway proteins by Western blotting across all four groups (Fig 6). Phosphorylated PI3K (p-PI3K) was significantly reduced in the SONFH group versus controls (Fig 6A and 6B; $P < 0.01$), and supplementation with either MMP-2 or Endostatin further decreased p-PI3K levels ($P < 0.05$), with no difference between the two supplementations. Similarly, both p-AKT and HIF-1 α were markedly lower in SONFH mice compared to controls (Fig 6C and 6D; $P < 0.001$), and supplementation

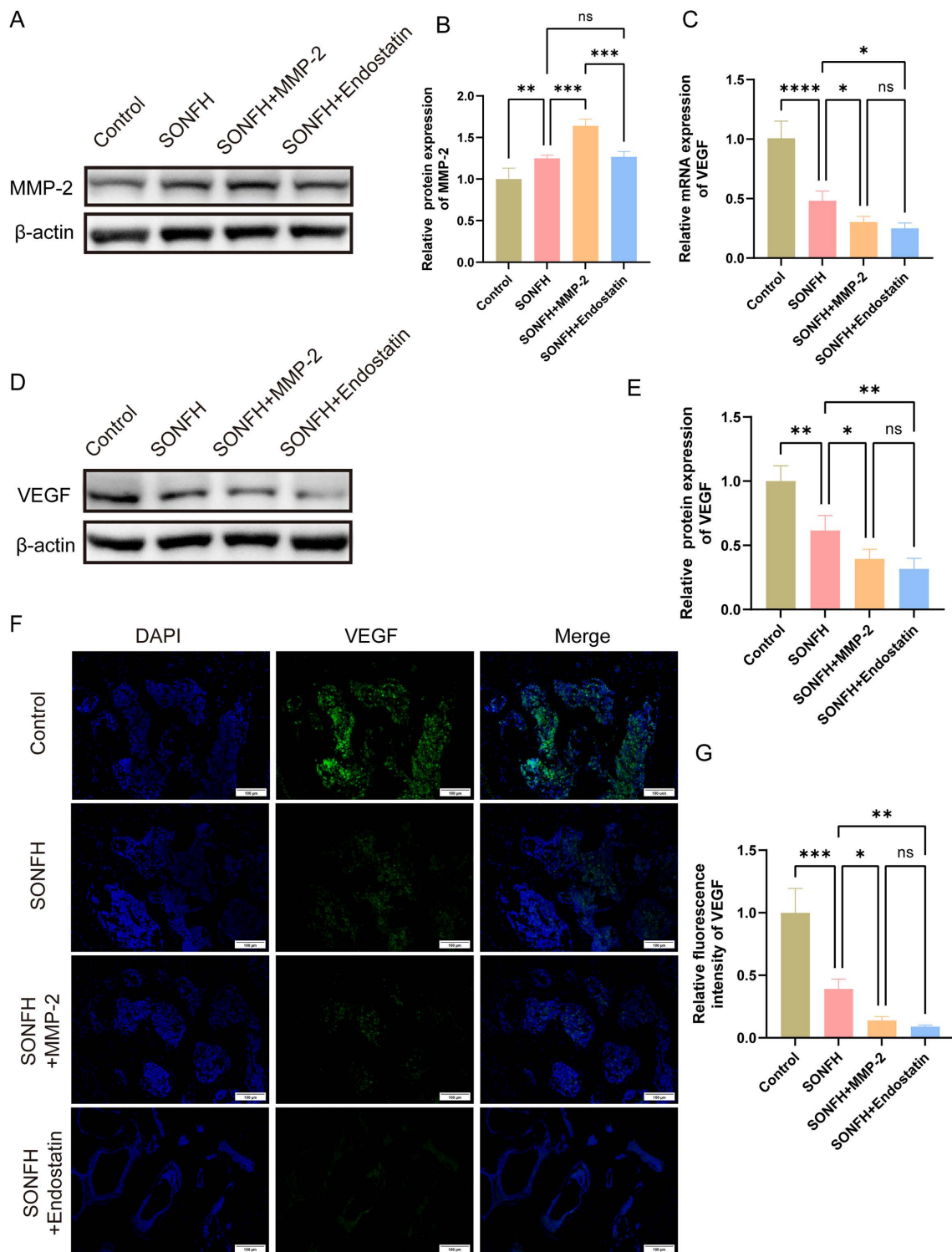


Fig 4. Influence of MMP-2 on VEGF expression. (A) Western blotting images showing MMP-2 protein expression; (B) Quantification of MMP-2 protein expression; (C) Relative mRNA levels of VEGF in the femoral head tissues of each group; (D) Western blotting images showing VEGF protein expression; (E) Quantification of VEGF protein expression; (F) Representative immunofluorescence images showing VEGF expression; (G) Quantitative analysis of VEGF immunofluorescence intensity. (* $P < 0.05$, ** $P < 0.01$, *** $P < 0.001$).

<https://doi.org/10.1371/journal.pone.0346880.g004>

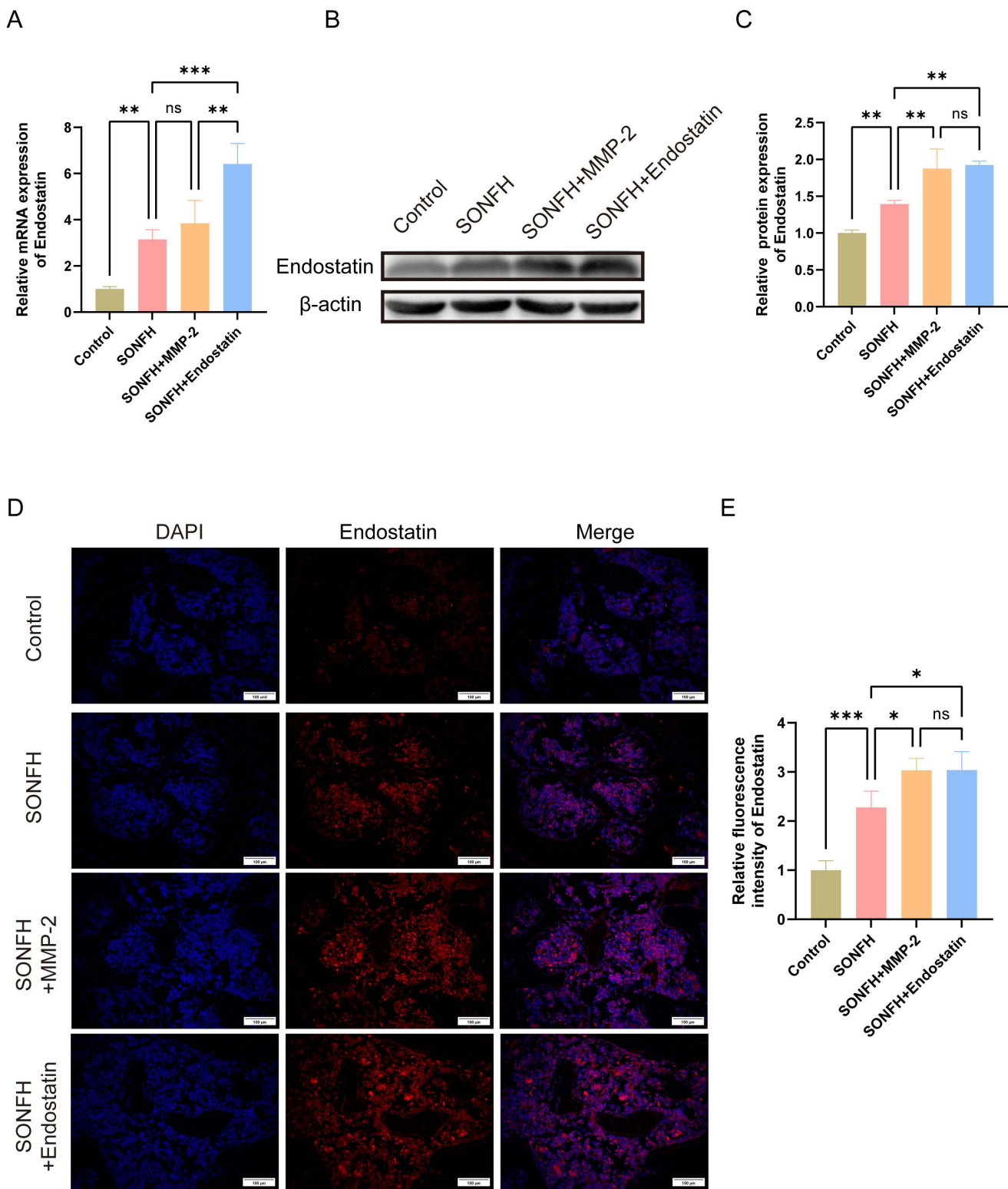


Fig 5. Effect of MMP-2 on Endostatin expression. (A) Relative mRNA levels of Endostatin in the femoral head tissues of each group; (B) Western blotting images showing Endostatin protein expression; (C) Quantification of Endostatin protein levels; (D) Representative immunofluorescence images of Endostatin expression; (E) Quantitative analysis of Endostatin immunofluorescence intensity. (* $P < 0.05$, ** $P < 0.01$, *** $P < 0.001$).

<https://doi.org/10.1371/journal.pone.0346880.g005>

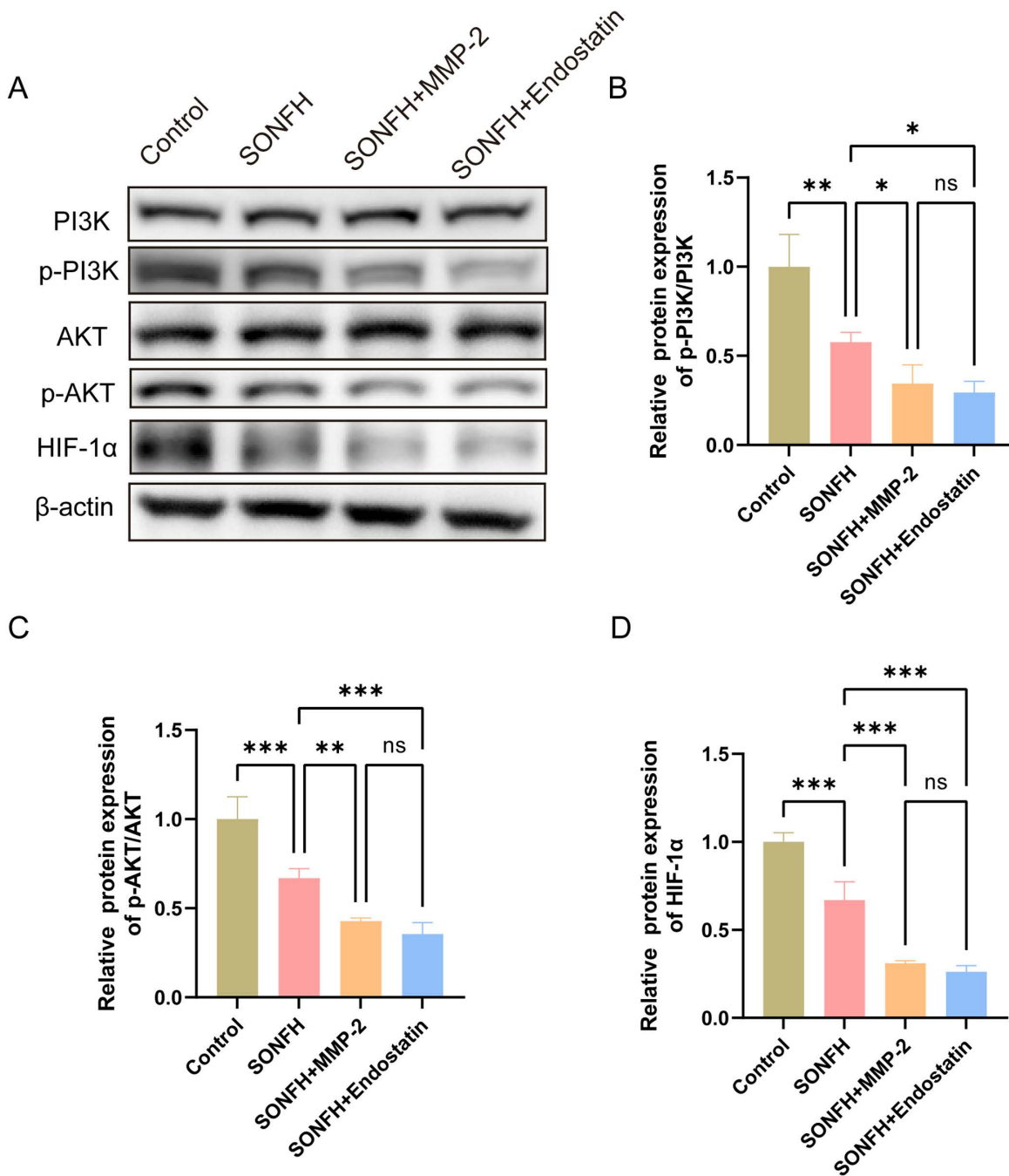


Fig 6. The expression of PI3K/AKT/HIF-1α axis in different experimental groups. (A) Western blotting images showing PI3K, AKT and HIF-1α protein expressions; (B) Quantification of p-PI3K protein levels; (C) Quantification of p-AKT protein levels; (D) Quantification of HIF-1α protein levels. (*P<0.05, **P<0.01, ***P<0.001).

<https://doi.org/10.1371/journal.pone.0346880.g006>

of MMP-2 or Endostatin caused additional reductions in p-AKT and HIF-1α ($P < 0.01$). The results indicate that glucocorticoid impairs the PI3K/AKT/HIF-1α axis in the femoral head and that both MMP-2 and Endostatin exacerbate this impairment.

4. Discussion

Osteonecrosis of the femoral head is characterized by interrupted blood supply to the femoral head, leading to ischemia, bone cell death, structural collapse, and ultimately the need for joint replacement. ONFH primarily affects individuals between 30 and 50 years of age, and it is estimated that 5% to 12% of total hip arthroplasty procedures are necessitated by ONFH [19]. Therefore, understanding the molecular regulation is critical to the development of early diagnostic markers and therapeutic strategies.

VEGF is a central pro-angiogenic factor that promotes endothelial proliferation, migration and vessel formation and is closely linked to osteogenesis. Previous studies report that VEGF augments both angiogenesis and bone formation in diverse repair models [20,21]. Endostatin, a collagen-XVIII derived endogenous angiogenesis inhibitor, counteracts VEGF-mediated endothelial responses and has been shown to suppress angiogenesis in bone healing contexts [22]. The physical exercise was shown to increase skeletal muscle VEGF expression while suppressing Endostatin expression, and a negative correlation was observed between Endostatin levels and capillary density [23]. Moreover, altered VEGF/Endostatin balance contributes to impaired angiogenesis in systemic sclerosis, and both of them can be biomarkers of systemic sclerosis [24,25]. Clinically, imbalances in VEGF and Endostatin expression have been linked to disease progression in melanoma, with stage III patients showing elevated Endostatin and reduced VEGF levels, while stage IV patients exhibited increased levels of both factors [26]. These findings suggest that the VEGF/Endostatin axis may serve not only as a therapeutic target but also as a potential biomarker for disease stage and severity.

Our study demonstrated that the VEGF/Endostatin ratio was significantly reduced in SONFH patients and mice. VEGF expression was downregulated, whereas Endostatin expression was increased. This imbalance suggests a shift toward an anti-angiogenic environment in the femoral head during SONFH progression. Importantly, although Figs 2 and 3 primarily depicts phenotypic outcomes, the subsequent analyses in Figs 4 and 5 demonstrate that Endostatin supplementation alters VEGF/Endostatin dynamics, decreasing VEGF levels while increasing Endostatin, which leads to a reduced VEGF/Endostatin ratio and provides a mechanistic explanation for the observed changes in angiogenesis and osteogenesis. Collectively, these data indicate that dysregulation of the VEGF/Endostatin axis is closely associated with impaired femoral head repair in SONFH.

MMP-2 has been implicated in the regulation of angiogenic factors, but its effects appear context-dependent. It should be noted that MMP-2 is a matrix-associated protease whose biological functions are highly dependent on the extracellular matrix context, which may not be fully recapitulated in simplified *in vitro* systems [27–29]. Some reports link MMP-2 inhibition to reduced VEGF and impaired angiogenesis, while others show that MMP-2 suppression can increase VEGF availability and promote repair, indicating tissue and disease specific roles [30–34]. These divergent findings underscore the complex regulatory role of MMP-2 in angiogenesis. In our study, elevated MMP-2 levels were observed in clinical samples from SONFH patients. Similarly, in the SONFH animal model, increased MMP-2 was accompanied by decreased VEGF, increased Endostatin, and a reduced VEGF/Endostatin ratio, mirroring the clinical findings. And both MMP-2 and Endostatin correlated with suppression of PI3K/AKT/HIF-1 α signaling. Excess MMP-2 activity may cleave basement membrane collagen XVIII, increasing extracellular Endostatin. Although ECM degradation by MMP-2 can release matrix-bound VEGF, proteolytic processing may limit VEGF bioavailability [35]. Activation of the PI3K/AKT/HIF-1 α axis is known to upregulate VEGF expression [36]. In this study, increased Endostatin was associated with downregulation of PI3K/AKT/HIF-1 α and reduced VEGF. Previous reports have shown that Endostatin can decrease HIF-1 α expression [37,38]. Taken together, these results suggest that MMP-2 affects the VEGF/Endostatin ratio and is associated with the suppression of PI3K/AKT/HIF-1 α pathway. However, the precise molecular links among MMP-2, Endostatin and PI3K/AKT/HIF-1 α remain to be defined.

Current therapeutic strategies for early stage SONFH are limited and largely palliative. Our data suggest that restoring a favorable VEGF/Endostatin ratio either by enhancing VEGF, inhibiting Endostatin, or modulating MMP-2 may be a promising approach to improve neovascularization and osteogenesis. The drugs selectively inhibit Endostatin could be

developed to promote angiogenic repair in the early stages of SONFH. Moreover, the VEGF/Endostatin ratio itself may serve as a novel biomarker for early diagnosis, treatment monitoring, or prognostic prediction.

Despite these encouraging results, several limitations of this study should be acknowledged. First, although MMP-2 was associated with a disturbed VEGF/Endostatin balance and reduced PI3K/AKT/HIF-1 α signaling, causality was not established. To address this, we will integrate ECM-enriched in vitro models together with in vivo MMP-2 knockdown and overexpression approaches to determine whether modulation of MMP-2 directly regulates angiogenic signaling, VEGF/Endostatin balance, and SONFH related phenotypes. Second, it remains unclear to what extent Endostatin mediates the effects of MMP-2. In the subsequent analyses, Endostatin knockdown during MMP-2 overexpression and adding recombinant Endostatin after MMP-2 inhibition will be performed. These experiments will clarify how strongly MMP-2 induced deterioration depends on Endostatin. Another limitation of this study is that the analyses were performed on whole femoral head tissue, which contains multiple cell types and therefore reflects averaged signals rather than cell-type-specific changes. Future studies will employ cell-type-specific approaches, such as laser-capture microdissection, cell sorting, and spatial transcriptomics, to further clarify the underlying mechanisms.

5. Conclusion

In summary, our study demonstrates that the VEGF/Endostatin ratio is markedly reduced in SONFH, and that further disruption of this balance exacerbates impairments in both angiogenesis and osteogenesis. Moreover, MMP-2 affects this ratio and is linked to the suppression of PI3K/AKT/HIF-1 α pathway. These findings deepen our understanding of SONFH pathogenesis and identify new molecular targets for its diagnosis and treatment.

Supporting information

S1 Table. Primers for RT-qPCR.

(PDF)

S2 Table. Antibodies for WB and IF staining.

(PDF)

S1 File. Raw images.

(PDF)

S2 File. The minimal anonymized dataset necessary.

(XLSX)

Author contributions

Conceptualization: Guangyang Zhang.

Data curation: Guangyang Zhang.

Formal analysis: Zhaopu Jing, Jialin Liang.

Investigation: Zhaopu Jing.

Methodology: Guangyang Zhang, Qichun Song.

Software: Jialin Liang.

Validation: Zhaopu Jing.

Visualization: Leifeng Lv.

Writing – original draft: Guangyang Zhang.

Writing – review & editing: Xiaoqian Dang, Qichun Song.

References

- Shah KN, Racine J, Jones LC, Aaron RK. Pathophysiology and risk factors for osteonecrosis. *Curr Rev Musculoskelet Med*. 2015;8(3):201–9. <https://doi.org/10.1007/s12178-015-9277-8> PMID: [26142896](https://pubmed.ncbi.nlm.nih.gov/26142896/)
- Li W, Li W, Zhang W, Wang H, Yu L, Yang P, et al. Exogenous melatonin ameliorates steroid-induced osteonecrosis of the femoral head by modulating ferroptosis through GDF15-mediated signaling. *Stem Cell Res Ther*. 2023;14(1):171. <https://doi.org/10.1186/s13287-023-03371-y> PMID: [37400902](https://pubmed.ncbi.nlm.nih.gov/37400902/)
- Pietrogrande V, Marino V. Study of the circulation of the femoral head in some patients with arthritis deformans of the hip. *Reumatismo*. 1953;5(Suppl. 2):219–22. PMID: [13100797](https://pubmed.ncbi.nlm.nih.gov/13100797/)
- Zhang C, Ma J, Li M, Li XH, Dang XQ, Wang KZ. Repair effect of coexpression of the hVEGF and hBMP genes via an adeno-associated virus vector in a rabbit model of early steroid-induced avascular necrosis of the femoral head. *Transl Res*. 2015;166(3):269–80. <https://doi.org/10.1016/j.trsl.2015.03.003> PMID: [25843672](https://pubmed.ncbi.nlm.nih.gov/25843672/)
- Nagashima M, Asano G, Yoshino S. Imbalance in production between vascular endothelial growth factor and endostatin in patients with rheumatoid arthritis. *J Rheumatol*. 2000;27(10):2339–42. PMID: [11036826](https://pubmed.ncbi.nlm.nih.gov/11036826/)
- Apte RS, Chen DS, Ferrara N. VEGF in signaling and disease: beyond discovery and development. *Cell*. 2019;176(6):1248–64. <https://doi.org/10.1016/j.cell.2019.01.021> PMID: [30849371](https://pubmed.ncbi.nlm.nih.gov/30849371/)
- Katsube K, Bishop AT, Simari RD, Ylä-Herttuala S, Friedrich PF. Vascular endothelial growth factor (VEGF) gene transfer enhances surgical revascularization of necrotic bone. *J Orthop Res*. 2005;23(2):469–74. <https://doi.org/10.1016/j.orthres.2004.08.013> PMID: [15734264](https://pubmed.ncbi.nlm.nih.gov/15734264/)
- Méndez-Valdés G, Gómez-Hevia F, Lillo-Moya J, González-Fernández T, Abelli J, Cereceda-Cornejo A, et al. Endostatin and cancer therapy: a novel potential alternative to anti-VEGF monoclonal antibodies. *Biomedicines*. 2023;11(3):718. <https://doi.org/10.3390/biomedicines11030718> PMID: [36979697](https://pubmed.ncbi.nlm.nih.gov/36979697/)
- Zhao Y, Li D, Duan D-P, Song Q-C. The effect of endostatin on angiogenesis and osteogenesis of steroid-induced osteonecrosis of the femoral head in a rabbit model. *Acta Orthop Traumatol Turc*. 2022;56(3):178–86. <https://doi.org/10.5152/j.aott.2022.21248> PMID: [35703505](https://pubmed.ncbi.nlm.nih.gov/35703505/)
- Hu Y, Hu M, Shi G-L, Han Y, Li B-L. Imbalance between vascular endothelial growth factor and endostatin correlates with the prognosis of operable non-small cell lung cancer. *Eur J Surg Oncol*. 2014;40(9):1136–42. <https://doi.org/10.1016/j.ejso.2014.05.014> PMID: [24998915](https://pubmed.ncbi.nlm.nih.gov/24998915/)
- Joo YY, Jang JW, Lee SW, Yoo SH, Kwon JH, Nam SW, et al. Circulating pro- and anti-angiogenic factors in multi-stage liver disease and hepatocellular carcinoma progression. *Sci Rep*. 2019;9(1):9137. <https://doi.org/10.1038/s41598-019-45537-w> PMID: [31235729](https://pubmed.ncbi.nlm.nih.gov/31235729/)
- Ai J, Ma J, Chen ZQ, Sun JH, Yao K. An endostatin-lentivirus (ES-LV)-EPC gene therapy agent for suppression of neovascularization in oxygen-induced retinopathy rat model. *BMC Mol Cell Biol*. 2020;21(1):57. <https://doi.org/10.1186/s12860-020-00301-1> PMID: [32727534](https://pubmed.ncbi.nlm.nih.gov/32727534/)
- Tolstanova G, Deng X, Khomenko T, Garg P, Paunovic B, Chen L, et al. Role of anti-angiogenic factor endostatin in the pathogenesis of experimental ulcerative colitis. *Life Sci*. 2011;88(1–2):74–81. <https://doi.org/10.1016/j.lfs.2010.10.026> PMID: [21047522](https://pubmed.ncbi.nlm.nih.gov/21047522/)
- Gyenge M, Amagase K, Kunimi S, Matsuoka R, Takeuchi K. Roles of pro-angiogenic and anti-angiogenic factors as well as matrix metalloproteinases in healing of NSAID-induced small intestinal ulcers in rats. *Life Sci*. 2013;93(12–14):441–7. <https://doi.org/10.1016/j.lfs.2013.07.021> PMID: [23900029](https://pubmed.ncbi.nlm.nih.gov/23900029/)
- Olenich SA, Gutierrez-Reed N, Audet GN, Olfert IM. Temporal response of positive and negative regulators in response to acute and chronic exercise training in mice. *J Physiol*. 2013;591(20):5157–69. <https://doi.org/10.1113/jphysiol.2013.254979> PMID: [23878369](https://pubmed.ncbi.nlm.nih.gov/23878369/)
- Liu G, Cao R, Liu Q, Li H, Yan P, Wang K, et al. M2 macrophages-derived exosomes for osteonecrosis of femoral head treatment: modulating neutrophil extracellular traps formation and endothelial phenotype transition. *Bone Res*. 2025;13(1):42. <https://doi.org/10.1038/s41413-025-00412-5> PMID: [40169566](https://pubmed.ncbi.nlm.nih.gov/40169566/)
- Yamamoto T, Saito O, Shono K, Ohtori S, Ino H. Analgesic effect of intrathecally administered matrix metalloproteinase 2 (MMP-2) in the rat formalin test. *Neurosci Lett*. 2003;347(2):77–80. [https://doi.org/10.1016/s0304-3940\(03\)00668-2](https://doi.org/10.1016/s0304-3940(03)00668-2) PMID: [12873732](https://pubmed.ncbi.nlm.nih.gov/12873732/)
- Azevedo A, Prado AF, Issa JPM, Gerlach RF. Matrix metalloproteinase 2 fused to GFP, expressed in *E. coli*, successfully tracked MMP-2 distribution in vivo. *Int J Biol Macromol*. 2016;89:737–45. <https://doi.org/10.1016/j.ijbiomac.2016.05.013> PMID: [27156693](https://pubmed.ncbi.nlm.nih.gov/27156693/)
- Zalavras CG, Lieberman JR. Osteonecrosis of the femoral head: evaluation and treatment. *J Am Acad Orthop Surg*. 2014;22(7):455–64. <https://doi.org/10.5435/JAAOS-22-07-455> PMID: [24966252](https://pubmed.ncbi.nlm.nih.gov/24966252/)
- Zha Y, Li Y, Lin T, Chen J, Zhang S, Wang J. Progenitor cell-derived exosomes endowed with VEGF plasmids enhance osteogenic induction and vascular remodeling in large segmental bone defects. *Theranostics*. 2021;11(1):397–409. <https://doi.org/10.7150/thno.50741> PMID: [33391482](https://pubmed.ncbi.nlm.nih.gov/33391482/)
- Allbritton-King JD, Maity J, Patel A, Colbert RA, Navid F, Bhattacharyya T. VEGF secretion drives bone formation in classical MAP2K1+ melorheostosis. *J Bone Miner Res*. 2023;38(12):1834–45. <https://doi.org/10.1002/jbmr.4915> PMID: [37737377](https://pubmed.ncbi.nlm.nih.gov/37737377/)
- Myren M, Kirby DJ, Noonan ML, Maeda A, Owens RT, Ricard-Blum S. Biglycan potentially regulates angiogenesis during fracture repair by altering expression and function of endostatin. *Matrix Biol*. 2016;52–54:141–50. <https://doi.org/10.1016/j.matbio.2016.03.008> PMID: [27072616](https://pubmed.ncbi.nlm.nih.gov/27072616/)

23. Gu J-W, Shparago M, Tan W, Bailey AP. Tissue endostatin correlates inversely with capillary network in rat heart and skeletal muscles. *Angiogenesis*. 2006;9(2):93–9. <https://doi.org/10.1007/s10456-006-9035-z> PMID: [16791708](https://pubmed.ncbi.nlm.nih.gov/16791708/)
24. Mangoni AA, Zinellu A. Endostatin as a biomarker of systemic sclerosis: insights from a systematic review and meta-analysis. *Front Immunol*. 2024;15:1450176. <https://doi.org/10.3389/fimmu.2024.1450176> PMID: [39763677](https://pubmed.ncbi.nlm.nih.gov/39763677/)
25. Zinellu A, Mangoni AA. Vascular endothelial growth factor as a potential biomarker in systemic sclerosis: a systematic review and meta-analysis. *Front Immunol*. 2024;15:1442913. <https://doi.org/10.3389/fimmu.2024.1442913> PMID: [39669565](https://pubmed.ncbi.nlm.nih.gov/39669565/)
26. Kurschat P, Eming S, Nashan D, Krieg T, Mauch C. Early increase in serum levels of the angiogenesis-inhibitor endostatin and of basic fibroblast growth factor in melanoma patients during disease progression. *Br J Dermatol*. 2007;156(4):653–8. <https://doi.org/10.1111/j.1365-2133.2006.07724.x> PMID: [17263813](https://pubmed.ncbi.nlm.nih.gov/17263813/)
27. Wolosowicz M, Prokopiuk S, Kaminski TW. The complex role of matrix metalloproteinase-2 (MMP-2) in health and disease. *Int J Mol Sci*. 2024;25(24):13691. <https://doi.org/10.3390/ijms252413691> PMID: [39769454](https://pubmed.ncbi.nlm.nih.gov/39769454/)
28. Piwocka O, Sterzyńska K, Malińska A, Suchorska WM, Kulcenty K. Development of tetraculture spheroids as a versatile 3D model for personalized breast cancer research. *Sci Rep*. 2025;15(1):27449. <https://doi.org/10.1038/s41598-025-12556-9> PMID: [40721466](https://pubmed.ncbi.nlm.nih.gov/40721466/)
29. Majo S, Redoute-Timonnier C, Lacour A, Challeat L, Epinette E, Teillon J, et al. Optimized zymogram protocol from 3D spheroid cultures to study MMP-2 and -9 activities in tumor cells. *BMC Biotechnol*. 2025;25(1):28. <https://doi.org/10.1186/s12896-025-00961-x> PMID: [40217226](https://pubmed.ncbi.nlm.nih.gov/40217226/)
30. Gam D-H, Park J-H, Kim J-H, Beak D-H, Kim J-W. Effects of *Allium sativum* stem extract on growth and migration in Melanoma cells through inhibition of VEGF, MMP-2, and MMP-9 genes expression. *Molecules*. 2021;27(1):21. <https://doi.org/10.3390/molecules27010021> PMID: [35011253](https://pubmed.ncbi.nlm.nih.gov/35011253/)
31. Gho Y, Shin S-S, Choi YH, Ko K, Kim W-J, Moon S-K. Hydrangenol suppresses VEGF-stimulated angiogenesis by targeting p27KIP1-dependent G1-cell cycle arrest, VEGFR-2-mediated signaling, and MMP-2 expression. *Anim Cells Syst (Seoul)*. 2019;23(2):72–81. <https://doi.org/10.1080/19768354.2019.1578262> PMID: [30949393](https://pubmed.ncbi.nlm.nih.gov/30949393/)
32. Bueno G, Chavez Rico SL, Périco LL, Ohara R, Rodrigues VP, Emilio-Silva MT, et al. The essential oil from *Baccharis trimera* (Less.) DC improves gastric ulcer healing in rats through modulation of VEGF and MMP-2 activity. *J Ethnopharmacol*. 2021;271:113832. <https://doi.org/10.1016/j.jep.2021.113832> PMID: [33460758](https://pubmed.ncbi.nlm.nih.gov/33460758/)
33. Kon M, Ebi Y, Nakagaki K. Hormonal, metabolic, and angiogenic responses to all-out sprint interval exercise under systemic hyperoxia. *Growth Horm IGF Res*. 2022;63:101445. <https://doi.org/10.1016/j.ghir.2022.101445> PMID: [35168036](https://pubmed.ncbi.nlm.nih.gov/35168036/)
34. Bonet A, Valença A, Mendes-Jorge L, Casellas A, Rodríguez-Baeza A, Nacher V, et al. Decreased endostatin in db/db retinas is associated with optic disc intravitreal vascularization. *Exp Eye Res*. 2021;212:108801. <https://doi.org/10.1016/j.exer.2021.108801> PMID: [34688624](https://pubmed.ncbi.nlm.nih.gov/34688624/)
35. Lee S, Jilani SM, Nikolova GV, Carpizo D, Iruela-Arispe ML. Processing of VEGF-A by matrix metalloproteinases regulates bioavailability and vascular patterning in tumors. *J Cell Biol*. 2005;169(4):681–91. <https://doi.org/10.1083/jcb.200409115> PMID: [15911882](https://pubmed.ncbi.nlm.nih.gov/15911882/)
36. Lin H, Wang X, Li Z, Huang M, Feng J, Chen H, et al. Total flavonoids of *Rhizoma drynariae* promote angiogenesis and osteogenesis in bone defects. *Phytother Res*. 2022;36(9):3584–600. <https://doi.org/10.1002/ptr.7525> PMID: [35960140](https://pubmed.ncbi.nlm.nih.gov/35960140/)
37. Zhao M-Z, Zheng H-F, Wang J-N, Zhang Y-M, Wang H-J, Zhao Z-W. Inhibitory effect of Endostar on HIF-1 with upregulation of MHC-I in lung cancer cells. *Cancer Biol Ther*. 2025;26(1):2508535. <https://doi.org/10.1080/15384047.2025.2508535> PMID: [40392714](https://pubmed.ncbi.nlm.nih.gov/40392714/)
38. Guo L, Chen Y, He T, Qi F, Liu G, Fu Y, et al. Nuclear-translocated endostatin downregulates hypoxia inducible factor-1 α activation through interfering with Zn(II) homeostasis. *Mol Med Rep*. 2015;11(5):3473–80. <https://doi.org/10.3892/mmr.2015.3223> PMID: [25607980](https://pubmed.ncbi.nlm.nih.gov/25607980/)